Prediction of H 2 S solubility in aqueous NaCl solutions by molecular simulation

Rémi Fauve, Xavier Guichet, Véronique Lachet, Nicolas Ferrando

Prediction of H$_2$S solubility in aqueous NaCl solutions by molecular simulation

Rémi Fauve[1], Xavier Guichet[1], Véronique Lachet[1,2], Nicolas Ferrando[1,*]

[1] IFP Energies nouvelles, 1 et 4 avenue de Bois-Préau, 92852 Rueil-Malmaison, France

[2] Laboratoire de Chimie Physique, Université Paris-Sud, UMR 8000 CNRS, Orsay, France

Abstract

The solubility of hydrogen sulfide in aqueous NaCl solutions has been investigated by calculation of Henry constants through Monte Carlo simulations and using a nonpolarizable force field. The Lorentz-Berthelot combining rules appeared the most appropriate to simulate this system compared to other usual rules. The physical behavior and the trends experimentally observed are qualitatively well reproduced by this purely predictive approach for the binary system H$_2$S+H$_2$O as well as for the salted system H$_2$S+H$_2$O+NaCl: as experimentally expected, the simulations indicate a maximum in the Henry constant curve with temperature and an increase of the Henry constant with the salt concentration (salting-out effect). From a quantitative point of view, Henry constants are systematically overestimated, and more specifically for high temperatures. By introducing an empirical temperature-independent binary interaction coefficient between water and hydrogen sulfide, it is possible to obtain a good agreement between experiments and calculated Henry constants for both salt-free and salted systems, over a large temperature range (290 to 590 K) and salinity ranging from 0 to 6 mol/kg. For temperatures less than 400 K, the deviations are smaller and within the experimental uncertainties. At higher temperatures, deviations are higher but only few experimental data are available to confirm this result. Considering statistical and experimental uncertainties, this approach can thus provide a reasonable estimation of H$_2$S solubility in NaCl aqueous solution in conditions encountered in geological formations. For a given temperature, the variation of the Henry constant with salt concentration is not exactly the same as the variation experimentally observed, and the salting-out effect is overestimated. This suggests for future works that additional forces such as polarization have to be taken into account for modeling high salt concentration systems.

Keywords: hydrogen sulfide; NaCl; solubility; Henry constant; Monte Carlo simulation

---

* Corresponding author : nicolas.ferrando@ifpen.fr

1. Introduction

Hydrogen sulfide (H_2S), produced in natural geological formation by the thermo-reduction of the sulfates (TSR), presents serious hazards when liberated in important quantities. The separation of H_2S from methane and other hydrocarbons is an important step in the treatment of a natural gas at the production site before transport, and represents important costs. The petroleum industry is therefore interested by the assessment of the reservoir H_2S content at the beginning of the exploration phase. To properly address the H_2S transport in geological formations, the dissolved amount of H_2S in formation waters has to be estimated. To calculate phase equilibrium of H_2S + brine systems, actually most of the available basin or reservoir modeling tools use empirical correlations (e.g. Barta and Bradley, 1985; Savary et al., 2012; Suleimenov and Krupp, 1994), activity coefficient models (e.g. Barrett et al., 1988; Dubessy et al., 2005; Li et al., 2014; Xia et al., 2000) or equations of state (e.g. Duan et al., 1996; Duan et al., 2007; Li et al., 2015; Soreide and Whitson, 1992; Ziabakhsh-Ganji and Kooi, 2012; Zirrahi et al., 2012). Such models require a large number of experimental data to be calibrated. A recent compilation (Koschel et al., 2013) indicates that around 700 experimental data of H_2S solubility in NaCl aqueous solutions are available in literature (Barrett et al., 1988; Douabul and Riley, 1979; Drummond, 1981; Kozintseva, 1963; Savary et al., 2012; Suleimenov and Krupp, 1994; Xia et al., 2000), but three quarters of them are for pressures less than 5 MPa. Actually the maximum experimental pressure investigated for H_2S solubility in brine is close to 30 MPa (Koschel et al., 2013; Savary et al., 2012), and the temperatures investigated are in a large majority less than 393 K, very far from conditions encountered in geological formations where TSR is expected to occur (Machel, 2001). Due to high toxicity and corrosiveness of this gas, experiments at high pressure are hazardous and expensive. Alternatives to experiments are thus recommended to evaluated H_2S solubility in severe temperature and pressure conditions.

For many years, molecular simulation has become a powerful tool to predict phase equilibrium of systems of industrial interest through Monte Carlo simulation techniques (Theodorou, 2010; Ungerer et al., 2005). The physical properties of aqueous electrolyte solutions have been widely studied in molecular simulation, and two kinds of force fields are commonly used: polarizable force fields and non-polarizable force fields. Using polarizable force fields to simulate water+salt systems (e.g. Jiang et al., 2015; Jiang et al., 2016; Kiss et al., 2012b; Kiss et al., 2012a; Kiss and Baranyai, 2014; Lamoureux and Roux, 2006; Moučka et al., 2013, 2015; Neyt et al., 2013; Rick et al., 1994; Yu et al., 2010) allows a better representation of interactions between centers of force and is expected to improve quantitative accuracy, but this approach is time consuming. Non-polarizable force fields have the benefit of greater simplicity and helps to save computation time for this system (e.g. Lísal et al., 2005; Mester and Panagiotopoulos, 2015; Moucka et al., 2013; Orozco et al., 2014). Although the water+salt system has been widely investigated in molecular simulation, the simulation of gas solubility in aqueous electrolyte solutions remains scarce and challenging due to high complexity of molecular interactions involving ionic species. Prior studies on this topic mainly concern CO_2 solubility in NaCl or $CaCl_2$ solutions (Liu et al., 2013; Tsai et al., 2016; Vorholz et al., 2004). To the best of our knowledge, no study dealing with the H_2S solubility in aqueous electrolyte solution by molecular simulation has been published in open literature. Hence, the goal of this work is to evaluate existing non-polarizable force fields and methodologies to predict H_2S solubility in aqueous NaCl solutions from 0 to 6 mol/kg by Monte Carlo simulations, and to identify the actual limitations of the evaluated approach. In the first part of this paper, a review of available experimental data on

75 both salt-free and salted systems is carried out and optimized parameters are proposed to correlate
76 these data. The second part deals with the molecular models and the combining rules used for the
77 simulations, and with the simulation techniques employed to compute the Henry constants of H_2S in
78 pure and salted water. The results obtained either for the binary system H_2S+H_2O or the ternary
79 system $H_2S+H_2O+NaCl$ are discussed in the third part. Conclusions and perspectives are provided in
80 the last section.

81

2. Review of available experimental data

2.1 The binary system H_2S+H_2O

84 For the binary system H_2S+H_2O, literature provides a large number of experimental data, mainly
85 given either in terms of Henry constant H_i (Rinker and Sandall, 2000), or in terms of H_2S solubility x_i
86 (molar fraction) (Barrett et al., 1988; Burgess and German, 1969; Chapoy et al., 2005; Gerrard, 1972;
87 Koschel et al., 2007; Kuranov et al., 1996; Lee and Mather, 1977; Pohl, H. A., 1961; Selleck et al.,
88 1952; Suleimenov and Krupp, 1994; Yu et al., 1980). At infinite dilution ($x_i \rightarrow 0$), the solubility and
89 the Henry constant are linked by the following relationship:

$$90 \quad H_i = \frac{f_i^{vap}}{x_i} = \frac{p_i \varphi_i^{vap}}{x_i} \qquad (1)$$

91 Where f_i^{vap} is the fugacity of the solute in the vapor phase, p_i is its partial pressure and φ_i^{vap} its
92 fugacity coefficient in the vapor phase.

93 In this work, all the experimental data have been gathered in terms of H_2S Henry constant in water.
94 Experimental data provided in terms of molar fraction have been converted in Henry constant using
95 equation (1), and the Soave-Redlich-Kwong equation of state (Soave, 1972) to estimate the vapor
96 fugacity coefficient of pure H_2S. To evaluate the experimental uncertainty, a correlation is used to
97 smooth these experimental data. Harvey (Harvey, 1996) proposed a widely used correlation involving
98 the critical temperature and the vapor pressure of water. We propose to use in this work the
99 extension of the Harvey correlation proposed by Trinh et al. (Trinh et al., 2016) which allows a better
100 extrapolation at high temperature:

$$101 \quad T_r \ln \frac{H_i}{P_{solvent}^{\sigma}} = a_i + b_i \left(1 - T_r\right)^{0.355} + c_i T_r \left(\frac{1}{T_r} - 1\right)^{1.5} \qquad (2)$$

102 where $P_{solvent}^{\sigma}$ is the pure water vapor pressure, and $T_r = T/T_c$ the water reduced temperature, with
103 T_c=647.096 K the critical temperature of water. The empirical parameters a_i, b_i and c_i are adjusted on
104 all experimental data (158 points ranging from 273.15 to 563.15 K), and are provided in Table 1.

105 Figure 1 shows the raw experimental data and the adjusted correlation. The average deviation
106 between experimental and smoothed data is about ±25% and that can be considered as an order of
107 magnitude of the experimental uncertainties. A maximum of the Henry constant is observed for T =
108 450 K. The number of experimental measurements decreases with increasing temperature, so that

3

109 experimental values are scarce for temperatures higher than 500 K. This correlation and its
110 uncertainty will be used for further comparisons with simulation results.

111

2.2 The ternary system H₂S+H₂O+NaCl

113 Experimental data of Henry constant or solubility of H₂S in aqueous NaCl solutions are mainly
114 provided at atmospheric pressure and low temperature (Barrett et al., 1988), far from conditions
115 encountered in natural geological formations. Some data are available at higher temperatures, such
116 as solubility measured by Koschel *et al.* (Koschel et al., 2013) (up to 353.15 K and 5 mol/kg for
117 salinity), Xia *et al.* (Xia et al., 2000) (up to 393.15 K and 6 mol/kg for salinity) and Henry constants
118 reported by Suleimenov *et al.* (Suleimenov and Krupp, 1994) (from 428 to 593 K and salinity up to 2
119 mol/kg). Experiments show that the solubility of H₂S tends to decrease when salt is added in the
120 system: this is the well-known salting-out effect. This effect is often correlated using an empirical
121 function $f\left(T, m_{sel}\right)$ linking the solubility of the gas in the salt-free system x_i and the solubility of
122 the gas in the salted system x_i^* :

123 $$\ln \frac{x_i}{x_i^*} = f\left(T, m_{salt}\right) \qquad (3)$$

124 Where m_{salt} stands for the salt molality (mol/kg of solvent).

125 One of the most widely function used is the Setschenow form (Setschenow, 1889), providing a linear
126 dependency of the logarithm of the solubility ratio with the salt concentration:

127 $$\ln \frac{x_i}{x_i^*} = k_s m_{salt} \qquad (4)$$

128 where k_s is the Setschenow coefficient.

129 However, some preliminary attempts to correlate the available experimental data with this simple
130 equation showed that a more complex function should be used to obtain a satisfactory accuracy.
131 Since the solubility ratio is related to the change in activity observed when salt is added in the
132 system, we propose in this work to use a correlation inspired from the Drummond's activity
133 coefficient model developed for neutral species in brines (Drummond, 1981):

134 $$\ln \frac{x_i}{x_i^*} = \left(C + F \cdot T + \frac{G}{T}\right) m_{salt} - \left(E + H \cdot T\right)\left(\frac{m_{salt}}{m_{salt}+1}\right) \qquad (5)$$

135 Where *C*, *F*, *G*, E and *H* are empirical parameters equal to -1.0312, 0.0012806, 255.9, 0.4445
136 and -0.001606, respectively, in the original work. In order to obtain the best possible agreement,
137 parameters C and E are refitted considering all the experimental data available for temperatures
138 ranging from 298 to 428 K, pressures less than vapor pressure of the solvent and salinity values up to
139 6 mol/kg. In these conditions of moderate pressures, the gas phase behaves like an ideal gas, and the
140 fugacity coefficient in equation (1) can be taken equal to 1. For an experimental value of $x_{H_2S}^*$, the

4

141 corresponding value of x_{H_2S} in pure water at the same temperature and partial pressure is calculated

142 from equation (1) and (2). The optimal values found for parameters C and E are equal to -1.113 and

143 0.3576, respectively. Figure 2 shows parity diagram between experimental data and calculated data

144 with equation (5).

145 Finally, for a given H₂S partial pressure and at infinite dilution, Henry constants and solubilities in salt-

146 free and salted systems are related by:

147 $$\frac{H_i^*}{H_i} = \frac{x_i}{x_i^*} \qquad (6)$$

148 Since the experimental data are scarce for temperatures greater than 400 K and for particularly high

149 salinity brine (greater than 1 mol/kg), the Henry constant in salted systems will be assessed by using

150 equations (5) and (6) and will be used as reference data to evaluate results obtained from molecular

151 simulation.

152

3. Simulation methods

153

3.1 Force field

154

155 The molecular model used for hydrogen sulfide is the model of Kristof and Liszi (Kristof and Liszi,

156 1997) which involves one Lennard-Jones center and four electrostatic charges. This model allows to

157 obtain a good accuracy for prediction of vapor pressures, saturated liquid densities and vaporization

158 enthalpies of pure H₂S (Kristof and Liszi, 1997; Ungerer et al., 2004). For water, the SPC/E model

159 (Berendsen et al., 1987) is used since prior studies showed good results in the prediction of aqueous

160 electrolyte properties with this model (Ji et al., 2012; Tsai et al., 2016). For Na⁺ and Cl⁻ ions, the OPLS

161 model is used (Chandrasekhar et al., 1984). This choice is motivated by the fact that when coupled

162 with the SPC/E model of water, this combination gives a reasonable prediction of the solution density

163 on a large range of temperature (from 298 to 548 K). The densities calculated for NaCl molality of 1, 3

164 and 5 mol/kg in the NPT ensemble are plotted on Figure 3, and the average deviations between

165 calculated and experimental density data (Apelblat and Manzurola, 1999; Romankiw and Chou, 1983;

166 Zhang and Han, 1996) is equal to 1%.

167 Finally, the Table 2 provides details of the molecular models used.

168 As molecules are assumed to be rigid, only intermolecular interactions are accounted for in the

169 potential energy calculation. Dispersion-repulsion interactions between force centers *i* and *j* are

170 modeled with a 6-12-Lennard-Jones potential with a spherical cut-off equal to the half of the

171 simulation box, and the classical tail correction is employed (Allen and Tildesley, 1987) :

172 $$U_{ij}^{LJ} = 4\varepsilon_{ij} \left[\left(\frac{\sigma_{ij}}{r_{ij}} \right)^{12} - \left(\frac{\sigma_{ij}}{r_{ij}} \right)^{6} \right] \qquad (7)$$

173 Where r_{ij} is the distance between the two force centers and ε_{ij} and σ_{ij} the energy and diameter

174 parameters of the Lennard-Jones potential, respectively.

5

175 The electrostatic energy between two charges *i* and *j* is modeled with a Coulomb potential:

176 $$U_{ij}^{el} = \frac{q_i q_i}{4\pi\varepsilon_0 r_{ij}} \qquad (8)$$

177 Where ε_0 is the vacuum permittivity. For long-range corrections, the Ewald summation technique is
178 used, with a number of reciprocal vectors k ranging from -7 to 7 in all three directions and a Gaussian
179 width α equal to 2 in reduced units. Finally, no explicit polarization interactions are considered in this
180 force field.

181 For the calculation of the cross Lennard-Jones parameters ε_{ij} and σ_{ij}, the Lorentz-Berthelot
182 combining rules have been used for interactions between ions + water and ions + H_2S. For the
183 interactions between water and H_2S, three usual combining rules (Lorentz-Berthelot, Kong (Kong,
184 1973) and Waldmann-Hagler (Waldmann and Hagler, 1993)), described in Table 3, are evaluated in
185 this work on the phase equilibrium calculation of the binary system H_2S + H_2O. This choice is
186 motivated by the fact that the Lorentz-Berthelot combining rules are widely used in molecular
187 simulation, and the Kong and Waldmann-Hagler combining rules yielded good accuracy in phase
188 equilibrium of systems involving light gases (Delhommelle and Millie, 2001; Ungerer et al., 2004;
189 Waldmann and Hagler, 1993).

190 As discussed later, an empirical correction of the Lorentz-Berthelot combining rule is also possible by
191 introducing a binary interaction parameter k_{ij}, generally adjusted to minimize the deviations between
192 experimental and calculated selected properties:

193 $$\varepsilon_{ij} = \sqrt{\varepsilon_i \varepsilon_j} \cdot \left(1 - k_{ij}\right) \qquad (9)$$

194

3.2 Algorithms

195
196

197 By definition, the fugacity of a solute in a liquid phase f_i^{liq} is related to its chemical potential μ_i^{liq} by
198 the relation:

199 $$f_i^{liq} = f_i^0 \exp\left(\frac{\mu_i^{liq} - \mu_i^0}{RT}\right) \qquad (10)$$

200 Where the superscript *0* stands for the reference state, *R* is the ideal gas constant and *T* is the
201 temperature.

202 The choice of the reference state is fully arbitrary. In this work, the reference state (zero chemical
203 potential) corresponds to an hypothetical pure ideal gas of unit density (1 molecule per Å^3, i.e. a
204 density ρ^0=1.66·10^6 mol/m^3). The fugacity in this reference state f_i^0 is then equal to $\rho^0 RT$.

205 As the phase equilibrium condition imposes:

6

206 $f_i^{vap} = f_i^{liq}$ (11)

207 the Henry constant defined by equation (1) can be determined by:

208 $H_i = \dfrac{f_i^0}{x_i} \exp\left(\dfrac{\mu_i^{liq} - \mu_i^0}{RT}\right)$ (12)

209 Thus, the Henry constant can be calculated by molecular simulation with any simulation algorithm
210 allowing the evaluation of the excess chemical potential $\mu_i^{ex} = \mu_i^{liq} - \mu_i^0$ of the solute in the liquid
211 phase.

212

3.2.1 Widom particle insertion algorithm
214

215 In this work, the first algorithm used to evaluate the chemical potential is the so-called Widom
216 particle insertion method (Frenkel and Smit, 1996; Widom, 1963), a smart algorithm allowing the
217 computation of the excess chemical potential through molecular simulations. In this method, the
218 excess chemical potential is calculated by the following ensemble average:

219 $\mu_i^{ex} = -k_B T \ln\left\langle \dfrac{PV}{k_B T (N+1)} \exp\left(-\dfrac{\Delta U}{k_B T}\right)\right\rangle_{NPT}$ (13)

220 Where k_B is the Boltzmann constant, ΔU is the potential energy difference due to the insertion of
221 the test molecule i, and T, P, V, and N are respectively the temperature, pressure, volume and
222 number of molecule in the system.

223 The Monte Carlo simulations are carried out in the NPT statistical ensemble. For each temperature
224 studied, the pressure of the system is taken equal to the vapor pressure of the solvent. For salt-free
225 systems, a total number of 520 water molecules is used. For salted system, the total number of water
226 molecules and ions is taken around 700, the number of Na$^+$ and Cl$^-$ ions being adjusted to obtain the
227 desired salt concentration in the liquid phase. The chemical potential is computed during a
228 production run lasting for typically 50 million and 100 million Monte Carlo steps in salt-free and
229 salted systems, respectively. One step corresponds to a single Monte Carlo move. Before each
230 production run, a preliminary run lasting for 50 (salt-free systems) to 100 (salted systems) million
231 Monte Carlo steps is carried out to achieve equilibrium. The different Monte Carlo moves and their
232 corresponding attempt probabilities used during simulations are molecular translation (20%),
233 molecular rotation (20%), volume change (0.5%) and insertion test (59.5%), with a preinsertion
234 statistical bias (Mackie et al., 1997). The amplitude of translations, rotations and volume changes are
235 adjusted during the simulation to achieve an acceptance ratio of 40%. The simulations were carried
236 out using the GIBBS software jointly developed by IFP Energies nouvelles and the Laboratoire de
237 Chimie Physique (CNRS-Université Paris-Sud) (Ungerer et al., 2005).

238

7

239 **3.2.2 Thermodynamic integration algorithm**

240

241 The simulations of the salted systems at high salt concentration yield to a dense and well-structured
242 liquid phase. From a simulation point of view, the insertion of a molecule of H_2S in the liquid phase
243 becomes more difficult and the convergence of a simulation longer to reach. In order to validate the
244 results obtained with the previous Widom insertion particle algorithm in the aqueous NaCl solutions,
245 the Henry constant of H_2S is also evaluated with an alternative method: the thermodynamic
246 integration algorithm (Frenkel and Smit, 1996). This method allows the computation of the Gibbs
247 energy of solvation of a solute ΔG_i^{solv} which is linked to the Henry constant of this solute by the
248 following relationship (Ben-Naim, 1978):

249 $$H_i = RT\rho_s^{liq} \exp\left(\frac{\Delta G_i^{solv}}{RT}\right) \qquad (14)$$

250 Where ρ_s^{liq} is the molar liquid density of the solvent. This method is based on a gradual insertion of
251 the solute in the solvent, avoiding thus the difficulties to insert directly a molecule in a dense phase.
252 However, as described below, this gradual insertion requires a large number of Monte Carlo
253 simulations for a single Henry constant computation. It is consequently an efficient but time-
254 consuming method. The thermodynamic integration algorithm has been extensively described
255 elsewhere (Economou et al., 2010; Garrido et al., 2009; Shirts et al., 2003), and only basics and
256 simulation details are given here. As the Gibbs energy is a state function, it can be calculated from a
257 thermodynamic cycle of non-physical transformations. Figure 4 describes the thermodynamic cycle
258 used to calculate the Gibbs energy of solvation, defined as the energy difference of the solute in
259 vacuum and in the solvent.

260 Following this cycle, the Gibbs energy of solvation is given by:

261 $$\Delta G^{solv} = \Delta G_{VdW}^{solvent} + \Delta G_{elec}^{solvent} + \Delta G^{dummy} - \Delta G^{vacuum} \qquad (15)$$

262

263 The terms $\Delta G_{VdW}^{solvent}$ and $\Delta G_{elec}^{solvent}$ correspond to the Gibbs energy of "insertion" of the bonded
264 assembly of uncharged Lennard-Jones spheres and to the Gibbs energy required for "charging" the
265 solute (Shirts et al., 2003). The term ΔG^{vacuum} corresponds to the same transformation, but in
266 vacuum instead of solvent. It thus involves only intramolecular interactions. As the molecules
267 considered in this work are rigid, this contribution is zero, as well as the contribution ΔG^{dummy} (Gibbs
268 energy of a non-interacting rigid molecule). The thermodynamic integration method consists in
269 evaluating a Gibbs energy difference using the following expression:

270

271 $$\Delta G = \int_0^1 \left\langle \frac{\partial U(\lambda)}{\partial \lambda} \right\rangle d\lambda \qquad (16)$$

272

273 where U is the interaction potential between solute and solvent, and λ a coupling variable: $\lambda = 1$
274 means a full coupling between the solute and the solvent molecules, while $\lambda = 0$ means that solute

8

275 does not interact with the solvent. As suggest by Beutler *et al.* (Beutler et al., 1994), a soft-core
276 potential for dispersion-repulsion interactions between solute and solvent molecules is used:

277

$$U_{ij}^{disp-rep} = 4\varepsilon_{ij}\lambda_{VdW}^n \left[\frac{1}{\left[\alpha\left(1-\lambda_{VdW}\right)^2 + \left(\frac{r_{ij}}{\sigma_{ij}}\right)^6 \right]^2} - \frac{1}{\alpha\left(1-\lambda_{VdW}\right)^2 + \left(\frac{r_{ij}}{\sigma_{ij}}\right)^6} \right]$$

278 (17)

279

280 Values of 0.5 and 4 are used for α and n, respectively (Shirts et al., 2003).

281

282 For the electrostatic energy the following coupling function is used (Chang, 2009; Garrido et al.,
283 2010; Partay et al., 2005; Shirts et al., 2003):

284

$$U_{ij}^{elec} = \frac{\lambda_C q_i q_j}{4\pi\varepsilon_0 r_{ij}}$$

285 (18)

286

287 As a charge overlap could generate a singularity, the calculation of electrostatic energy for the
288 various values of λ_C should be carried out for $\lambda_{VdW} = 1$ to ensure sufficient repulsion between atoms
289 bearing electrostatic charges. The complete methodology can be summarized as follows. First,
290 $\Delta G_{VdW}^{solvent}$ is calculated by fixing $\lambda_C = 0$ and by performing one Monte Carlo simulation per value of
291 λ_{VdW}. The following 16 values of λ_{VdW} are selected: {0, 0.1, 0.2, 0.3, 0.35, 0.4, 0.425, 0.45, 0.475, 0.5,
292 0.55, 0.6, 0.7, 0.8, 0.9, 1}. Second, ΔG_{elec}^{solv} is calculated by fixing $\lambda_{VdW} = 1$ and by performing one
293 Monte Carlo simulation per value of λ_C. The following 11 values of λ_C are selected: {0, 0.1, 0.2, 0.3,
294 0.4, 0.5, 0.6, 0.7, 0.8, 0.9, 1}. A Monte Carlo simulation consists in simulating a NPT ensemble at the
295 desired temperature and the vapor pressure of the solvent, with one molecule of solute, and a total
296 of around 700 molecules of water and ions. A simulation run lasted for 200 million steps, including an
297 equilibrium run of 100 million steps. The different Monte Carlo moves and their corresponding
298 attempt probabilities used during the simulations are molecular translation (50%), molecular rotation
299 (49.5%), and volume change (0.5%).

300

4. Results and discussion

301
302

4.1 The binary system $H_2S + H_2O$

303
304

305 The simulation results obtained from Widom test insertion method with the three different
306 combining rules (Lorentz-Berthelot, Kong and Waldmann-Hagler) are plotted on Figure 5. This figure
307 clearly exhibits that the combining rules of Kong and Waldmann-Hagler strongly overestimate the

308 Henry constant of H_2S in pure water, and are not suitable to model this system accurately. Using the
309 Lorentz-Berthelot rules also tends to overestimate experimental Henry constant but with a reduced
310 deviation (average relative deviation of around 50%). This deviation remains higher than the
311 estimated experimental uncertainties but it is worth noticing that with this purely predictive
312 approach the variation of the Henry constant with temperature is qualitatively well reproduced, and
313 more specifically the existence of a maximum at around 450 K.

314 For engineering needs, more quantitative results could be required. The use of an empirical binary
315 interaction parameter k_{ij} in the Lorentz-Berthelot combining rule (equation (9)) is a possible way to
316 reduce deviations with experiments, although strongly altering the predictive feature of the
317 molecular simulation approach. A temperature-independent k_{ij} is adjusted on experimental Henry
318 constant data, leading to an optimal value of -0.16. The simulations with this empirical parameter
319 lead to average deviation of around 40%, still higher than experimental uncertainties. As illustrated
320 on Figure 6, the calculated Henry constant with this optimal k_{ij} are underevaluated at low
321 temperature and overestimated at high temperature. Thus, the appropriate empirical correction
322 would be to introduce a temperature-dependent k_{ij}, and the following linear dependency has been
323 optimized on experimental data:

324 $$k_{ij}(T) = -4.43 \cdot 10^{-4} \cdot T(K) + 0.103 \qquad (19)$$

325 In this case, the average deviation decreases to 19%, but the simulations are in no way predictive,
326 and this approach will be no more considered further. To obtain a better accuracy with a fully
327 predictive way, the force field has to be drastically modified. As Henry constant is overestimated (and
328 consequently solubility underestimated), it could also be argued that neglecting the dissociation of
329 H_2S into HS^- and S^{2-} in our modeling approach is not a correct assumption. However, considering an
330 average dissociation constant of $9.6 \cdot 10^{-8}$ for the first acidity (Sun et al., 2008) , the concentration of
331 HS^- remains less than 1% of the concentration of dissolved molecular H_2S for pH up to 5.5, and this
332 cannot reasonably explain the overestimation observed.

333
334

4.2. The ternary system H_2S + H_2O + NaCl

336

337 The addition of salt makes the aqueous phase more dense and more structured due to the solvation
338 of ions by the water molecules. This behavior can be visualized on the radial distribution functions
339 (rdf) between H_2O-Na^+ pairs and H_2O-Cl^- pairs plotted on Figure 7. These rdf exhibit two large peaks
340 at 2.4 and 3.3 Å, respectively, indicating a high probability to find water molecules at this short
341 distance of ions. The integration of the denormalized rdf (coordination numbers) gives a total
342 number of 6 water molecules surrounding a Na^+ ion and of 7 water molecules surrounding a Cl^- ion in
343 the first solvation shell, determined by the location of the first minima in the rdf. This result is
344 consistent with previous simulation studies (Impey et al., 1983; Lee and Rasaiah, 1996). Increasing
345 temperature tends to decrease the coordination number due to thermal agitation. A decrease of
346 about 10% in the coordination number of both Na^+ and Cl^- is observed by changing the temperature
347 from 298 K to 548 K.

10

348   Figure 8 compares the Henry constants at 323.15 K and salinities from 0 to 5 mol/kg calculated using
349   either the Widom test insertion method or the thermodynamic integration algorithm. Results
350   obtained using the same force field are found very close and lie within the statistical uncertainties of
351   these two methods (typically between +/-5 and +/-10 % for Widom test insertion and +/- 10 and
352   +/- 20% for thermodynamic integration). For further calculations, the Widom particle insertion
353   method will be systematically used since it allows a direct calculation of Henry constant in a single
354   Monte Carlo simulation.

355   Figure 9 shows the variation of Henry constant of H_2S in a NaCl aqueous solution for three molal
356   concentrations as a function of temperature. The Monte Carlo simulation results obtained with the
357   predicted approach without k_{ij} are in green, while the ones obtained with the approach using the
358   optimized H_2S-H_2O k_{ij} are in blue. For each molality, the available experimental data are plotted (red
359   dots). The dash line is the correlated Henry constant of H_2S in pure water (eq. 2). The bold line is the
360   correlated Henry constant of H_2S in aqueous solutions calculated according the approach described
361   in section 2.2. The shaded grey area shows the minimal uncertainty associated to the experimental
362   measurements.

363   The Monte Carlo simulation results obtained with the predicted approach clearly overestimate the
364   Henry constants. The overestimation increases with increasing temperature (typically above 400 K),
365   and with increasing salinity of the aqueous solution. It can be noticed that at high temperatures, only
366   few experimental data are available. New experimental data could be useful to confirm or not this
367   behavior. As shown in figure 1, our model underestimates densities at high temperature. But as an
368   underestimation of density should theoretically lead to an underestimation of Henry constant, this
369   cannot explain the overestimation observed. When using the previous optimal k_{ij} for the binary
370   system H_2S+H_2O (k_{ij}=-0.16), results for the ternary system are found with a better quantitative
371   agreement but remain overestimated at high temperatures (above 450 K)., As for the salt-free
372   systems, experimental data exhibit a maximum, but shifted toward higher temperatures (above 500
373   K). The simulations are able to reproduce this behavior, with a maximum predicted close to 500 K.

374   Figure 10 shows the evolution of the H_2S Henry constant as a function of NaCl concentration for
375   three isotherms (323.15, 353.15 and 393.15 K). Experimental data exhibit an increase of the Henry
376   constant (and consequently a decrease of H_2S solubility) when salt concentration increases. This is
377   the well-known "salting-out" effect, and simulation results qualitatively reproduce this behavior.
378   Nevertheless the predictive approach without k_{ij} overestimates this effect, and more specifically at
379   high salt concentration (above 3 mol/kg). The Henry constants obtained by Monte Carlo simulations
380   with the approach using the optimized H_2S-H_2O k_{ij} are in fairly good agreement with the experimental
381   data and this regardless the molality of the aqueous solution.

382   From a quantitative point of view, Table 4 provides for each temperature the average deviations
383   obtained with both approaches evaluated. Without the binary interaction parameter, deviations are
384   quite large, and this predictive approach has to be used only to estimate trends. When using the
385   optimized H_2S-H_2O interaction coefficient, average deviations are reduced and of the same order of
386   magnitude as the experimental uncertainties. Thus, considering the experimental and statistical
387   uncertainties, this last approach allows to obtain a reasonable estimation of H_2S solubility in brines.

388   It makes clear that at high salt concentration, this nonpolarizable model fails to correctly describe the
389   complex interactions in the electrolyte solution. The negative value for the k_{ij} indicates that the

11

390 attraction forces between H_2S and H_2O are presently underestimated. This suggests that attraction
391 forces are missing in the force field, and a future improvement could consist in taking into account
392 explicitly polarization forces. Furthermore, the effect of polarization forces will be more pronounced
393 in high salt concentration solutions. The polarization energies due to cation P_+ and anion P_- in a
394 solvent can be evaluated with (Misztal and Sangwal, 1999):

395 $$P = P_+ + P_- = -\frac{1}{2}e^2\left(1-\frac{1}{\varepsilon}\right)\left(\frac{1}{R_+} + \frac{1}{R_-}\right) \qquad (20)$$

396 With e is the elementary charge ($e = 1.062 \cdot 10^{-19}$ C), R_+ and R_- are the solvated ion radii in the solvent
397 of dielectric constant ε. For Na^+, the solvated ionic radius is taken equal to 0.2356 ± 0.006 nm, and for
398 Cl^-, the solvated radius is taken equal to 0.3187 ± 0.0025 nm (Marcus, 1988). The static dielectric
399 constant for aqueous NaCl solutions is expected to decrease with increasing ionic concentrations (for
400 instance at 25°C, the dielectric constant decreases from 78 to 35 for ionic concentrations increasing
401 from 0 to 6 mol/kg) (Wang and Anderko, 2001). The evaluation of the polarization energy due to
402 cations and anions in a NaCl aqueous solution, according to equation (20) for two temperatures (273
403 K and 323 K), as a function of the ionic concentration is shown in Figure 11. The magnitude of
404 polarization energy is increasing linearly with the NaCl concentration, and is little affected by the
405 temperature.

406 Figure 12 shows the radial distribution functions for Na^+-Cl^- ionic pairs in NaCl aqueous solutions for
407 molalities ranging from 1 to 5 mol/kg. It clearly appears that the radial distribution exhibits a
408 maximum around 2.9 Å for molalities greater than 3 mol/kg indicating the formation of ionic pairs in
409 the solution. This behavior is consistent with observations made in prior studies on ion pairing in
410 NaCl aqueous solutions (see e.g. (Chen and Pappu, 2007; Lyubartsev and Laaksonen, 1996)). It can be
411 also generalized to other chloride salts, such as LiCl (e.g. (Chialvo and Simonson, 2007; Degreve and
412 Mazzé, 2003), KCl (Chen and Pappu, 2007) or $CaCl_2$ (Megyes et al., 2006). The formation of these
413 ionic pairs seems strongly affect the assessment of the Henry constant with the predictive approach,
414 but has a lesser effect for the approach using the optimized H_2S-H_2O k_{ij}. This last observation may be
415 linked to the behavior of the static dielectric constant with the salinity of NaCl solutions. For instance
416 at 298 K, the static dielectric constant decreases strongly from 78 to ca. 45 for salinity ranging from 0
417 to 3 mol/kg, it decreases only from 45 to ca. 35 for salinity ranging from 3 to 6 mol/kg. The overall
418 decrease of the static dielectric constant is linked to the formation of solvation layers (by water
419 molecules). For aqueous solutions, the formation of hydration shells around ions prevents the
420 "bound" water molecule from being oriented in the external electric field, thus causing a decrease of
421 the dielectric constant. A further increase in the salt concentration (from 3 to 6 mol/kg) leads to a
422 water deficit and to a redistribution of water molecules in the hydration shells, this levels off the
423 decrease of the dielectric constant (Wang and Anderko, 2001).

424 All these observations seem to indicate that the use of a constant k_{ij} is well adapted to take into
425 account the first order of the polarization corrections.

426

427

12

428 # 5. Conclusions

429

430 In this work, the solubility of hydrogen sulfide in aqueous NaCl solutions has been investigated by
431 calculation of Henry constant through Monte Carlo simulations and Widom particle insertion
432 method. A nonpolarizable force field is used, involving the SPC/E molecular model for water, the
433 Kriztof and Liszi model for H_2S and the OPLS model for Na^+ and Cl^-. For the binary system H_2S+H_2O,
434 the Lorentz-Berthelot combining rules appeared the most appropriate to simulate this system
435 compared to other usual rules (Kong and Waldmann-Hagler). The physical behavior and the trends
436 experimentally observed are qualitatively well reproduced by this purely predictive approach for the
437 binary system H_2S+H_2O as well as for the salted system $H_2S+H_2O+NaCl$. Experimental data indicate a
438 maximum in the Henry constant curve with temperature, close to 450 K for salt-free system and
439 500 K in an aqueous NaCl solution at 1 mol/kg, and the location of this maximum is well predicted by
440 the simulations. Moreover, the "salting-out" effect experimentally observed is also predicted by our
441 calculations. However, from a quantitative point of view, Henry constants are systematically
442 overestimated, and more specifically for high temperatures. By introducing an empirical
443 temperature-independent binary interaction coefficient between water and hydrogen sulfide, it is
444 possible to obtain a quite good agreement between experiments and calculated Henry constants for
445 both salt-free and salted systems, over a large temperature range (290 to 590 K) and salinity ranging
446 from 0 to 6 mol/kg. For temperatures less than 400 K, the deviations are smaller and within the
447 experimental uncertainties. At higher temperatures, deviations are higher but only few experimental
448 data are available to confirm this result. Considering statistical and experimental uncertainties, this
449 approach can thus provide a reasonable estimation of H_2S solubility in NaCl aqueous solution in
450 conditions encountered in geological formations. For a given temperature, the variation of the Henry
451 constant with salt concentration is not exactly the same as the variation experimentally observed,
452 and the salting-out effect remains overestimated. This suggests for future works that additional
453 forces such as polarization have to be taken into account for modeling high salt concentration
454 systems.

455

13

References

Allen, M.P., Tildesley, D.J., 1987. Computer Simulation of Liquids. Oxford University Press.

Apelblat, A., Manzurola, E., 1999. Volumetric properties of water, and solutions of sodium chloride and potassium chloride at temperatures fromT=277.15 K toT=343.15 K at molalities of (0.1, 0.5, and 1.0)mol. J.Chem.Thermodyn. 31 (7), 869–893.

Barrett, T.J., Anderson, G.M., Lugowski, J., 1988. The solubility of hydrogen sulphide in 0–5 m NaCl solutions at 25°–95°C and one atmosphere. Geochim.Cosmochim.Acta 52 (4), 807–811. 10.1016/0016-7037(88)90352-3.

Barta, L., Bradley, D.J., 1985. Extension of the specific interaction model to include gas solubilities in high temperature brines. Geochim.Cosmochim.Acta 49 (1), 195–203. 10.1016/0016-7037(85)90204-2.

Ben-Naim, A., 1978. A simple model for demonstrating the relation between solubility, hydrophobic interaction, and structural changes in the solvent. J. Phys. Chem. 82 (8), 874–885. 10.1021/j100497a007.

Berendsen, H.J.C., Grigera, J.R., Straatsma, T.P., 1987. The missing term in effective pair potentials. J. Phys. Chem. 91 (24), 6269–6271. 10.1021/j100308a038.

Beutler, T.C., Mark, A.E., Vanschaik, R.C., Gerber, P.R., Vangunsteren, W.F., 1994. Avoiding Singularities and Numerical Instabilities in Free-Energy Calculations Based on Molecular Simulations. Chemical Physics Letters 222 (6), 529–539.

Burgess, M.P., German, R.P., 1969. Physical Properties of Hydrogen Sulfide - Water Mixtures. AIChE J. 15, 272–275.

Chandrasekhar, J., Spellmeyer, D.C., Jorgensen, W.L., 1984. Energy component analysis for dilute aqueous solutions of lithium(1+), sodium(1+), fluoride(1-), and chloride(1-) ions. J. Am. Chem. Soc. 106 (4), 903–910. 10.1021/ja00316a012.

Chang, J., 2009. The calculation of chemical potential of organic solutes in dense liquid phases by using expanded ensemble Monte Carlo simulations. J.Chem.Phys. 131 (7).

Chapoy, A., Mohammadi, A.H., Tohidi, B., Valtz, A., Richon, D., 2005. Experimental measurement and phase behavior modeling of hydrogen sulfide-water binary system. Ind.Eng.Chem.Res. 44 (19), 7567–7574.

Chen, A.A., Pappu, R.V., 2007. Quantitative Characterization of Ion Pairing and Cluster Formation in Strong 1:1 Electrolytes. J. Phys. Chem. B 111 (23), 6469–6478. 10.1021/jp0708547.

Chialvo, A.A., Simonson, J.M., 2007. Ion pairing and counterion condensation in aqueous electrolyte and polyelectrolyte solutions: Insights from molecular simulation. EMLG/JMLG 2005 Special IssueAnnual Meeting of the EMLG/JMLG 2005 134 (1–3), 15–22. 10.1016/j.molliq.2006.12.017.

Degreve, L.É., Mazzé, F.M., 2003. Molecular simulation of LiCl aqueous solutions. Molecular Physics 101 (10), 1443–1453. 10.1080/0026897031000092256.

Delhommelle, J., Millie, P., 2001. Inadequacy of the Lorentz-Berthelot combining rules for accurate predictions of equilibrium properties by molecular simulation. Mol.Phys. 99, 619–625.

douabul, A.A., Riley, J.P., 1979. The Solubility of Gases in Distilled Water and Seawater - V. Hydrogen Sulfide. Deep-Sea Res. 26, 259–268.

Drummond, D., 1981. Boiling and Mixing of Hydrothermal Fluids: Chemical Effects on Mineral Precipitation. PhD Thesis, Pennsylvania State University, State College, PA.

Duan, Z., Moller, N., Weare, J.H., 1996. Prediction of the solubility of H2S in NaCl aqueous solution: an equation of state approach. Chem.Geol. 130, 15–20.

14

500 Duan, Z., Sun, R., Liu, R., Zhu, C., 2007. Accurate Thermodynamic Model for the Calculation of H2S
501   Solubility in Pure Water and Brines. Energy Fuels 21 (4), 2056–2065. 10.1021/ef070040p.

502 Dubessy, J., Tarantola, A., Sterpenich, J., 2005. Modelling of Liquid-Vapour Equilibria in the H2O-CO2-
503   NaCl and H2O-H2S-NaCl Systems to 270°C. Oil & Gas Science and Technology - Rev.IFP 60, 339–
504   355.

505 Economou, I.G., Garrido, N.M., Makrodimitri, Z.A., 2010. Prediction of microscopic structure and
506   physical properties of complex fluid mixtures based on molecular simulation. Fluid Phase Equilib.
507   296, 125–132. 10.1016/j.fluid.2010.09.040.

508 Frenkel, D., Smit, B., 1996. Understanding Molecular Simulation: From Algorithms to Applications.
509   Academic Press, San Diego.

510 Garrido, N.M., Queimada, A.J., Jorge, M., Economou, I.G., Macedo, E.A., 2010. Molecular simulation
511   of absolute hydration Gibbs energies of polar compounds. Fluid Phase Equilib. 296 (2), 110–115.

512 Garrido, N.M., Queimada, A.J., Jorge, M., Macedo, E.A., Economou, I.G., 2009. 1-Octanol/Water
513   Partition Coefficients of n-Alkanes from Molecular Simulations of Absolute Solvation Free
514   Energies. Journal of Chemical Theory and Computation 5 (9), 2436–2446.

515 Gerrard, W., 1972. Solubility of Hydrogen Sulfide, Dimethyl Ether, Methyl Chloride, and Sulfur
516   Dioxide in Liquids. The Prediction of Solubility of All Gases. J. Appl. Chem. Biotechnol. 22, 623–
517   650.

518 Harvey, A.H., 1996. Semiempirical correlation for Henry's constants over large temperature ranges.
519   AIChE J. 42, 1491–1494.

520 Impey, R.W., Madden, P.A., McDonald, I.R., 1983. Hydration and mobility of ions in solution: The
521   Journal of Physical Chemistry. The Journal of Physical Chemistry 87 (25), 5071–5083.
522   10.1021/j150643a008.

523 Ji, Q., Pellenq, R., van Vliet, K., 2012. Comparison of computational water models for simulation of
524   calcium–silicate–hydrate. Computational Materials Science 53 (1), 234–240.
525   10.1016/j.commatsci.2011.08.024.

526 Jiang, H., Mester, Z., Moultos, O.A., Economou, I.G., Panagiotopoulos, A.Z., 2015. Thermodynamic
527   and Transport Properties of H2O + NaCl from Polarizable Force Fields. J. Chem. Theory Comput.
528   11 (8), 3802–3810. 10.1021/acs.jctc.5b00421.

529 Jiang, H., Moultos, O.A., Economou, I.G., Panagiotopoulos, A.Z., 2016. Hydrogen-Bonding Polarizable
530   Intermolecular Potential Model for Water. J. Phys. Chem. B 120 (48), 12358–12370.
531   10.1021/acs.jpcb.6b08205.

532 Kiss, P.T., Baranyai, A., 2014. A new polarizable force field for alkali and halide ions. J.Chem .Phys.
533   141, 114501.

534 Kiss, P.T., Bertsyk, P., Baranyai, A., 2012a. Testing recent charge-on-spring type polarizable water
535   models. I. Melting temperature and ice properties. J.Chem .Phys. 137, 194102.

536 Kiss, P.T., Darvas, M., Baranyai, A., Jedlovszky, P., 2012b. Surface properties of the polarizable
537   Baranyai-Kiss water model. J.Chem .Phys. 136, 114706.

538 Kong, C.L., 1973. Combining rules for intermolecular potential parameters. II. Rules for the Lennard-
539   Jones (12-6) potential and the Morse potential. J.Chem.Phys. 59, 2464.

540 Koschel, D., Coxam, J.Y., Majer, V., 2013. Enthalpy and Solubility Data of H2S in Aqueous Salt
541   Solutions at Conditions of Interest for Geological Sequestration. Ind. Eng. Chem. Res. 52, 14483–
542   14491.

15

543   Koschel, D., Coxam, J.-Y., Majer, V., 2007. Enthalpy and Solubility Data of H2S in Water at Conditions
544   of Interest for Geological Sequestration. Ind. Eng. Chem. Res. 46 (4), 1421–1430.
545   10.1021/ie061180.

546   Kozintseva, T.N., 1963. Solubility of Hydrogen Sulfide in Water and on Salt Solutions at Elevated
547   Temperatures. In: Geokhimischskie issledovaniya v oblasti povyshennykh davlenii i temperatur.
548   Khitarova, N. I., Ed; Akademiia Nauk, Moscow.

549   Kristof, T., Liszi, J., 1997. Effective intermolecular potential for fluid hydrogen sulfide. J.Phys.Chem.B
550   101 (28), 5480–5483.

551   Kuranov, G., Rumpf, B., Smirnova, N.A., Maurer, G., 1996. Solubility of single gases carbon dioxide
552   and hydrogen sulfide in aqueous solutions of N-methyldiethanolamine in the temperature range
553   313-413 K at pressures up to 5 MPa. Ind.Eng.Chem.Res. 35 (6), 1959–1966.

554   Lamoureux, G., Roux, B., 2006. Absolute Hydration Free Energy Scale for Alkali and Halide Ions
555   Established from Simulations with a Polarizable Force Field. J. Phys. Chem. B 110 (7), 3308–3322.
556   10.1021/jp056043p.

557   Lee, J.I., Mather, A.E., 1977. Solubility of Hydrogen Sulfide in water. Berichte der Bunsen-Gesellschaft
558   f_r Physikalische Chemie 81 (10), 1021–1023.

559   Lee, S.H., Rasaiah, J.C., 1996. Molecular Dynamics Simulation of Ion Mobility. 2. Alkali Metal and
560   Halide Ions Using the SPC/E Model for Water at 25 -¦CÔÇá: The Journal of Physical Chemistry.
561   The Journal of Physical Chemistry 100 (4), 1420–1425. 10.1021/jp953050c.

562   Li, J., Wei, L., Li, X., 2014. Modeling of CO2-CH4-H2S-brine based on cubic EOS and fugacity-activity
563   approach and their comparisons. 12th International Conference on Greenhouse Gas Control
564   Technologies, GHGT-12 63, 3598–3607. 10.1016/j.egypro.2014.11.390.

565   Li, J., Wei, L., Li, X., 2015. An improved cubic model for the mutual solubilities of CO2–CH4–H2S–brine
566   systems to high temperature, pressure and salinity. Applied Geochemistry 54, 1–12.
567   10.1016/j.apgeochem.2014.12.015.

568   Lísal, M., Smith, W.R., Kolafa, J., 2005. Molecular Simulations of Aqueous Electrolyte Solubility: 1.
569   The Expanded-Ensemble Osmotic Molecular Dynamics Method for the Solution Phase. J. Phys.
570   Chem. B 109 (26), 12956–12965. 10.1021/jp0507492.

571   Liu, Y., Lafitte, T., Panagiotopoulos, A.Z., Debenedetti, P.G., 2013. Simulations of vapor–liquid phase
572   equilibrium and interfacial tension in the CO2–H2O–NaCl system. AIChE J. 59 (9), 3514–3522.
573   10.1002/aic.14042.

574   Lyubartsev, A.P., Laaksonen, A., 1996. Concentration Effects in Aqueous NaCl Solutions. A Molecular
575   Dynamics Simulation. J. Phys. Chem. 100 (40), 16410–16418. 10.1021/jp961317h.

576   MAchel, H.G., 2001. Bacterial and thermochemical sulfate reduction in diagenetic settings -old and
577   new insights. Sedimentary Geology 140, 143–175.

578   Mackie, A.D., Tavitian, B., Boutin, A., Fuchs, A.H., 1997. Vapour-liquid phase equilibria predictions of
579   methane-alkane mixtures by Monte Carlo simulation. Mol.Sim. 19 (1), 1–15.

580   Marcus, Y., 1988. Ionic radii in aqueous NaCl solutions. Chem.Rev. 88 (1475-1498).

581   Megyes, T., Bakó, I., Bálint, S., Grósz, T., Radnai, T., 2006. Ion pairing in aqueous calcium chloride
582   solution: Molecular dynamics simulation and diffraction studies. New Highlights of Solution
583   Chemistry: Diffraction, Simulation and Theoretical StudiesInvited Contributions Dedicated to
584   Professor Gabor Palinkas on Occasion on his 65th Birthday 129 (1–2), 63–74.
585   10.1016/j.molliq.2006.08.013.

586   Mester, Z., Panagiotopoulos, A.Z., 2015. Mean ionic activity coefficients in aqueous NaCl solutions
587   from molecular dynamics simulations. J.Chem .Phys. 142, 44507.

588 Misztal, R., Sangwal, K., 1999. Analysis of the Concentration and Temperature Dependence of
589   Densities of Aqueous Alkali Halide Solutions: a New Power-Law Approach. Crystal Research and
590   Technology 34, 769–775.
591 Moucka, F., Nezbeda, I., Smith, W.R., 2013. Molecular force fields for aqueous electrolytes: SPC/E-
592   compatible charged LJ sphere models and their limitations. J.Phys.Chem 138, 154102.
593 Moučka, F., Nezbeda, I., Smith, W.R., 2013. Computationally efficient Monte Carlo simulations for
594   polarisable models: multi-particle move method for water and aqueous electrolytes. Molecular
595   Simulation 39 (14-15), 1125–1134. 10.1080/08927022.2013.804183.
596 Moučka, F., Nezbeda, I., Smith, W.R., 2015. Chemical Potentials, Activity Coefficients, and Solubility in
597   Aqueous NaCl Solutions: Prediction by Polarizable Force Fields. J. Chem. Theory Comput. 11 (4),
598   1756–1764. 10.1021/acs.jctc.5b00018.
599 Neyt, J.-C., Wender, A., Lachet, V., Ghoufi, A., Malfreyt, P., 2013. Prediction of the concentration
600   dependence of the surface tension and density of salt solutions: atomistic simulations using
601   Drude oscillator polarizable and nonpolarizable models. Phys. Chem. Chem. Phys. 15 (28), 11679–
602   11690. 10.1039/C3CP50904D.
603 Orozco, G.A., Moultos, O.A., Jiang, H., Economou, I.G., Panagiotopoulos, A.Z., 2014. Molecular
604   simulation of thermodynamic and transport properties for H2O+NaCl system. J.Chem .Phys. 141,
605   234507.
606 Partay, L., Jedlovszky, P., Jancso, G., 2005. Calculation of the hydration free energy difference
607   between pyridine and its methyl-substituted derivatives by computer simulation methods. The
608   Journal of Physical Chemistry B 109 (16), 8097–8102.
609 Pohl, H. A., 1961. Thermodynamics of the Hydrogen Sulfide-Water-System Relevant to the Dual
610   Temperature Process for the Production of Heavy Water. J. Chem. Eng. Data 6 (4), 515–521.
611   10.1021/je60011a010.
612 Rick, S.W., Stuart, S.J., Berne, B.J., 1994. Dynamic fluctuating charge force fields: application to liquid
613   water. J.Chem .Phys. 101, 6141.
614 Rinker, E.B., Sandall, O.C., 2000. Physical solubility of hydrogen sulfide in several aqueous solvents.
615   Can.J.Chem.Eng. 78 (1), 232–236.
616 Romankiw, L.A., Chou, I.M., 1983. Densities of Aqueous Sodium Chloride, Potassium Chloride,
617   Magnesium Chloride, and Calcium Chloride Binary Solutions in the Concentration Range 0.5-6.1
618   M at 25, 30, 35, 40, and 45 C. J.Chem.Eng.Data 28 (3), 300–305.
619 Savary, V., Berger, G., Dubois, M., Lacharpagne, J.-C., Pages, A., Thibeau, S., Lescanne, M., 2012. The
620   solubility of CO2 + H2S mixtures in water and 2 M NaCl at 120 °C and pressures up to 35 MPa.
621   International Journal of Greenhouse Gas Control 10, 123–133. 10.1016/j.ijggc.2012.05.021.
622 Selleck, F.T., Carmichael, L.T., Sage, B.H., 1952. Phase behavior in the hydrogen sulfide-water system.
623   Ind.Eng.Chem.Res. 44 (9), 2219–2226.
624 Setschenow, J.Z., 1889. Uber die konstitution der saltzosungenauf grund ihres verhaltens zu
625   kohlensaure. Z.Physik.Chemie 4, 117–125.
626 Shirts, M.R., Pitera, J.W., Swope, W.C., Pande, V.S., 2003. Extremely precise free energy calculations
627   of amino acid side chain analogs: Comparison of common molecular mechanics force fields for
628   proteins. J.Chem.Phys. 119 (11), 5740–5761.
629 Soave, G., 1972. Equilibrium Constants for a Modified Redlich-Kwong Equation of State. Chemical
630   Engineering Science 27, 1197–1203.
631 Soreide, I., Whitson, C., 1992. Peng-Robinson predictions for hydrocarbons, CO_2, N_2, and H_2S with
632   pure water and NaCl brine. Fluid Phase Equilib. 77, 217–240.

633 Suleimenov, O.M., Krupp, R.E., 1994. Solubility of hydrogen sulfide in pure water and in NaCl
634   solutions, from 20 to 320°C and at saturation pressures. Geochim.Cosmochim.Acta 58 (11),
635   2433–2444. 10.1016/0016-7037(94)90022-1.

636 Sun, W., Nešić, S., Young, D., Woollam, R.C., 2008. Equilibrium Expressions Related to the Solubility of
637   the Sour Corrosion Product Mackinawite. Ind. Eng. Chem. Res. 47 (5), 1738–1742.
638   10.1021/ie070750i.

639 Theodorou, D.N., 2010. Progress and Outlook in Monte Carlo Simulations. Ind.Eng.Chem.Res. 49,
640   3047–3058.

641 Trinh, T.-K.-H., Hemptinne, J.-C. de, Lugo, R., Ferrando, N., Passarello, J.-P., 2016. Hydrogen Solubility
642   in Hydrocarbon and Oxygenated Organic Compounds. J. Chem. Eng. Data 61 (1), 19–34.
643   10.1021/acs.jced.5b00119.

644 Tsai, E.S., Jiang, H., Panagiotopoulos, A.Z., 2016. Monte Carlo simulations of H2O-CaCl2 and H2O-
645   CaCl2-CO2 mixtures. Fluid Phase Equilib. 407, 262–268.

646 Ungerer, P., Tavitian, B., Boutin, A., 2005. Applications of Molecular Simulation in the Oil and Gas
647   Industry. Editions Technip.

648 Ungerer, P., Wender, A., Demoulin, G., Bourasseau, E., Mougin, P., 2004. Application of Gibbs
649   Ensemble and NPT Monte Carlo Simulation to the Development of Improved Processes for H2S-
650   rich Gases. Mol.Sim. 30 (10), 631–648.

651 Vorholz, J., Harismiadis, V.I., Panagiotopoulos, A.Z., Rumpf, B., Maurer, G., 2004. Molecular
652   Simulation of the Solubility of Carbon Dioxide in Aqueous Solutions of Sodium Chloride. Fluid
653   Phase Equilib. 226, 237–250.

654 Waldmann, M., Hagler, A.T., 1993. New combining rules for rare gas van der waals parameters.
655   J.Comput.Chem. 14, 1077–1084.

656 Wang, P., Anderko, A., 2001. Computation of dielectric constants of solvent mixtures and electrolyte
657   solutions. Fluid Phase Equilib. 186, 103–122.

658 Widom, B., 1963. Some topics in the theory of fluids. J.Chem.Phys. 39, 2808–2812.

659 Xia, J., Pérez-Salado Kamps, Á., Rumpf, B., Maurer, G., 2000. Solubility of Hydrogen Sulfide in
660   Aqueous Solutions of the Single Salts Sodium Sulfate, Ammonium Sulfate, Sodium Chloride, and
661   Ammonium Chloride at Temperatures from 313 to 393 K and Total Pressures up to 10 MPa. Ind.
662   Eng. Chem. Res. 39 (4), 1064–1073. 10.1021/ie990416p.

663 Yu, H., Whitfield, T.W., Harder, E., Lamoureux, G., Vorobyov, I., Anisimov, V.M., MacKerell, A.D.,
664   Roux, B., 2010. Simulating Monovalent and Divalent Ions in Aqueous Solution Using a Drude
665   Polarizable Force Field. J. Chem. Theory Comput. 6 (3), 774–786. 10.1021/ct900576a.

666 Yu, Q., Liu, D., Liu, R., Zhou, H., Chen, M., Chen, G., Chen, Y., Hu, Y., Xu, X., Shen, L., Han, S.J., 1980.
667   VLE of H2S-H2O System. Huagong Xuebao 4, 1–7.

668 Zhang, Han, 1996. Viscosity and Density of Water + Sodium Chloride + Potassium Chloride Solutions
669   at 298.15 K. J. Chem. Eng. Data 41 (3), 516–520. 10.1021/je9501402.

670 Ziabakhsh-Ganji, Z., Kooi, H., 2012. An Equation of State for thermodynamic equilibrium of gas
671   mixtures and brines to allow simulation of the effects of impurities in subsurface CO2 storage.
672   CATO: CCS Research in the Netherlands 11, Supplement, S21-S34. 10.1016/j.ijggc.2012.07.025.

673 Zirrahi, M., Azin, R., Hassanzadeh, H., Moshfeghian, M., 2012. Mutual solubility of CH4, CO2, H2S,
674   and their mixtures in brine under subsurface disposal conditions. Fluid Phase Equilibria 324, 80–
675   93. 10.1016/j.fluid.2012.03.017.

18

Table 1. Parameters of correlation **Error! Reference source not found.** for the Henry constant of H_2S in pure water.

a_i	b_i	c_i
-1.67464	8.53988	-1.18646

Table 2. Details of molecular models used

Molecule	Force center or charge	Position (Å)			Lennard-Jones parameters		Charge
		X	Y	Z	σ (Å)	ε/k (K)	q (e)
H_2O	O	0	0	0	3.1655	78.2	-0.8476
	H1	0.8165	0.5774	0	0	0	0.4238
	H2	-0.8165	0.5774	0	0	0	0.4238
H_2S	S	0	0	0	3.7300	250.0	-0.4
	H1	0.9639	0.9308	0	0	0	0.25
	H2	-0.9639	0.9308	0	0	0	0.25
	M	0	0.1862	0	0	0	-0.9
Na^+	Na	0	0	0	1.8974	808.7	1
Cl^-	Cl	0	0	0	4.4172	59.3	-1

Table 3. Evaluated combining rules for the binary system H$_2$S + H$_2$O

Lorentz-Berthelot	Kong	Waldmann-Hagler
$\varepsilon_{ij} = \sqrt{\varepsilon_i \varepsilon_j}$ $\sigma_{ij} = \dfrac{\sigma_i + \sigma_j}{2}$	$\varepsilon_{ij}\sigma_{ij}^6 = \sqrt{\varepsilon_i\sigma_i^6 \varepsilon_j\sigma_j^6}$ $\varepsilon_{ij}\sigma_{ij}^{12} = \dfrac{\varepsilon_i\sigma_i^{12}}{2^{13}}\left[1+\left(\dfrac{\varepsilon_j\sigma_j^{12}}{\varepsilon_i\sigma_i^{12}}\right)^{\frac{1}{13}}\right]^{13}$	$\varepsilon_{ij}\sigma_{ij}^6 = \sqrt{\varepsilon_i\sigma_i^6 \varepsilon_j\sigma_j^6}$ $\sigma_{ij} = \left(\dfrac{\sigma_i^6 + \sigma_j^6}{2}\right)^{\frac{1}{6}}$

Table 4. Average deviations (%) between experimental (Koschel et al., 2013; Xia et al., 2000) and calculated H_2S Henry constants in NaCl aqueous solutions from 0 to 6 mol/kg.

T (K)	without k_{ij}	with k_{ij}(H_2S-H_2O) = -0.16
323.15	72.8	39.4
353.15	171.0	34.5
393.16	183.2	38.5
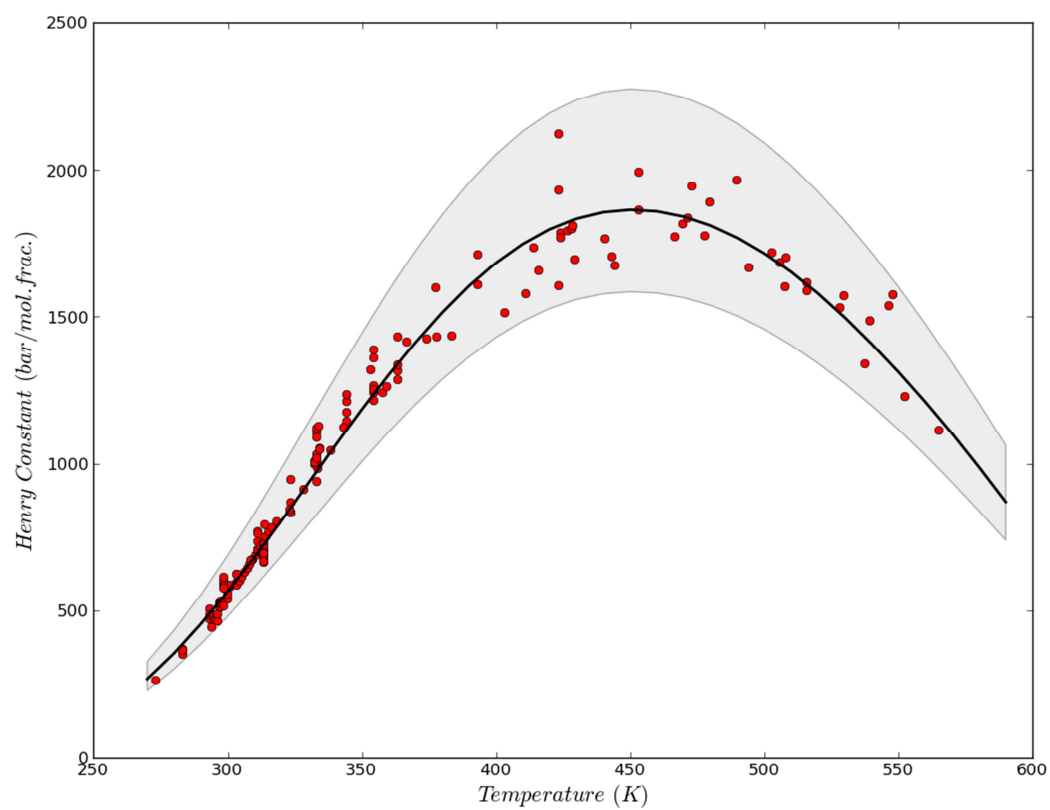
Figure 1. Experimental (symbols) and correlated (bold line) Henry constants of H₂S in pure water; the shaded grey area highlights the experimental uncertainties.

Henry Constants in brines
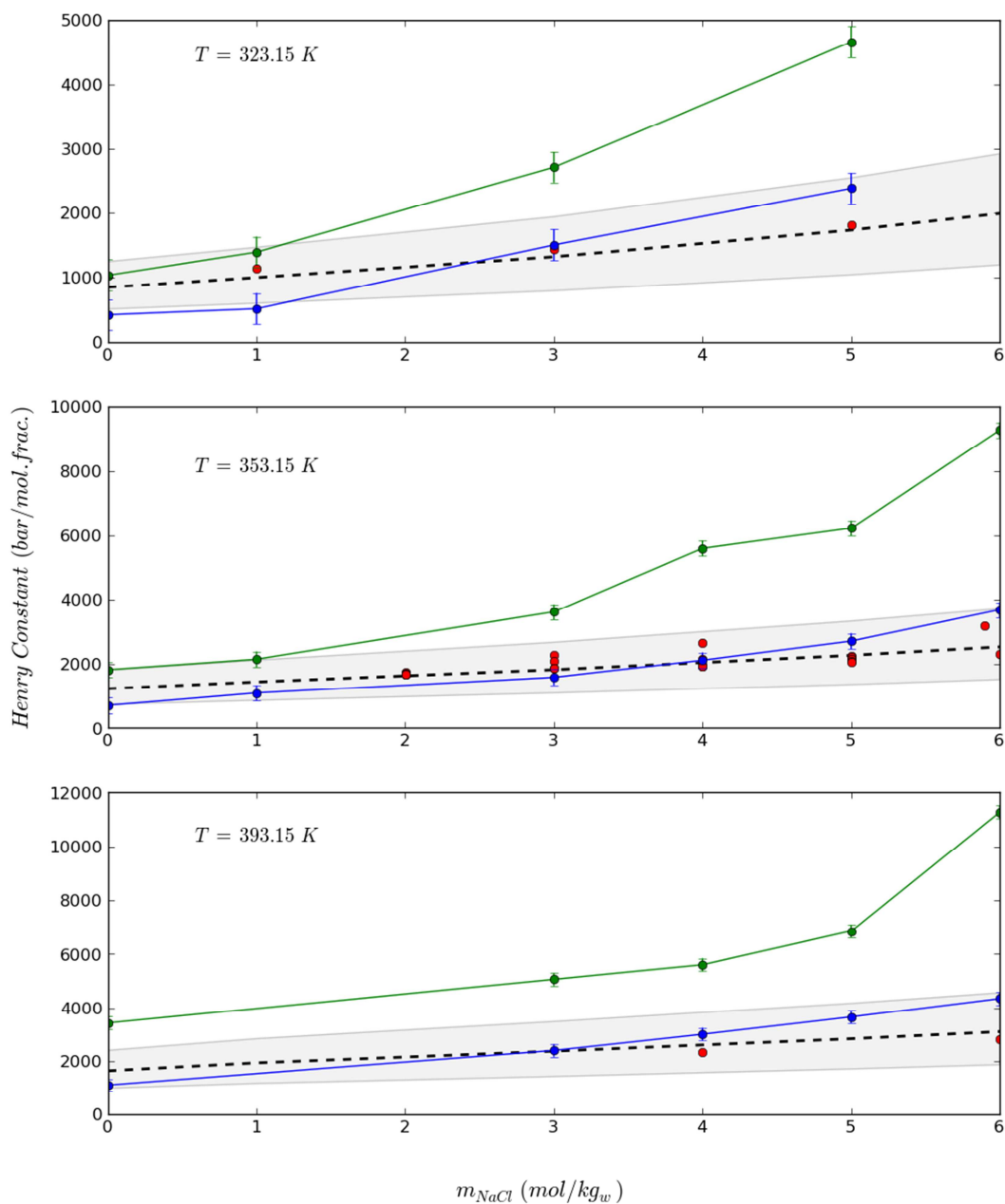
Figure 10. Henry constant of H_2S in NaCl aqueous solutions at 323.15 K (a), 353.15 K (b) and 393.15 K (c). The Monte Carlo simulation results obtained with the predicted approach without k_{ij} are in green, while the ones obtained with the approach using the optimized H_2S-H_2O k_{ij} are in blue. For each molality, the available experimental data are plotted (red dots). The dashed line is the correlated Henry constant of H_2S in aqueous solutions calculated according the approach described in section 2.2. The shaded grey area shows the minimal uncertainty associated to the experimental measurements.
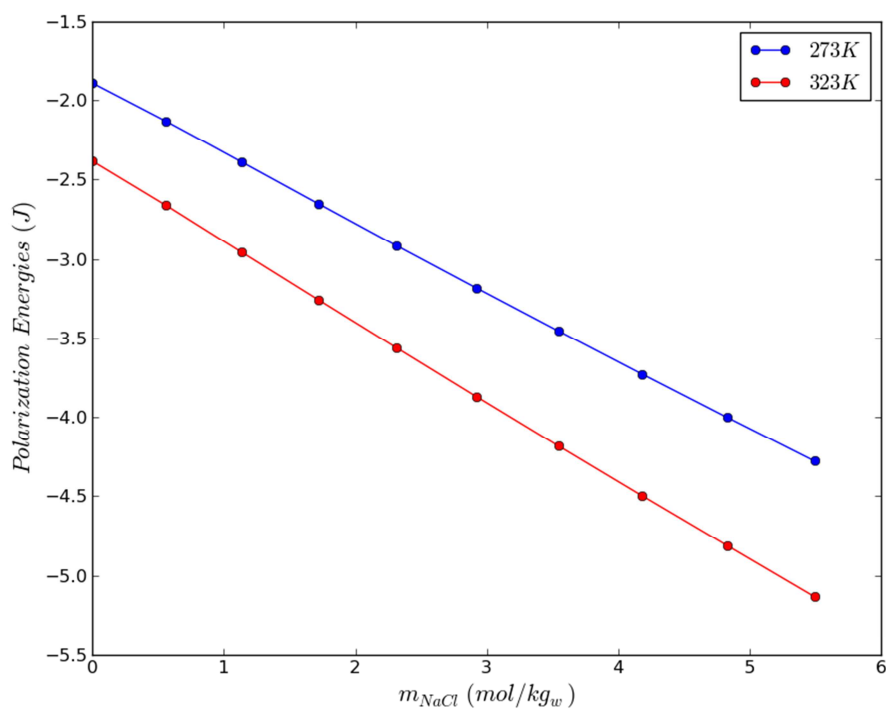
Figure 11. Assessment of the polarization energy due to cations and anions in a NaCl aqueous solution as a function of the ionic concentration at 273 K and 323 K

Interatomic distances
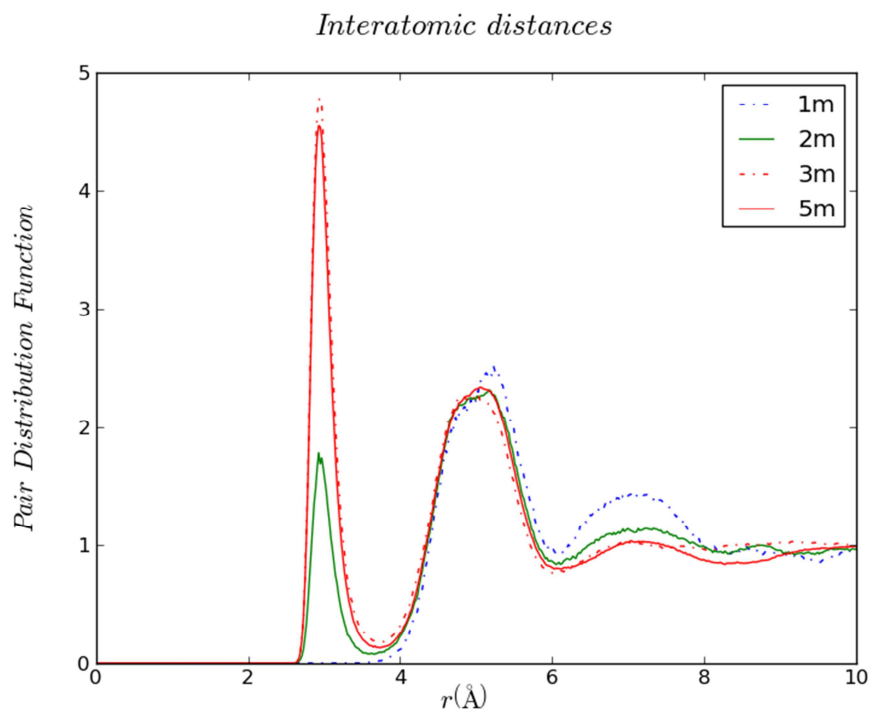
Figure 12. Radial distribution functions for Na$^+$-Cl$^-$ ionic pairs in a NaCl aqueous solution for molality ranging from 1 to 5 mol/kg.
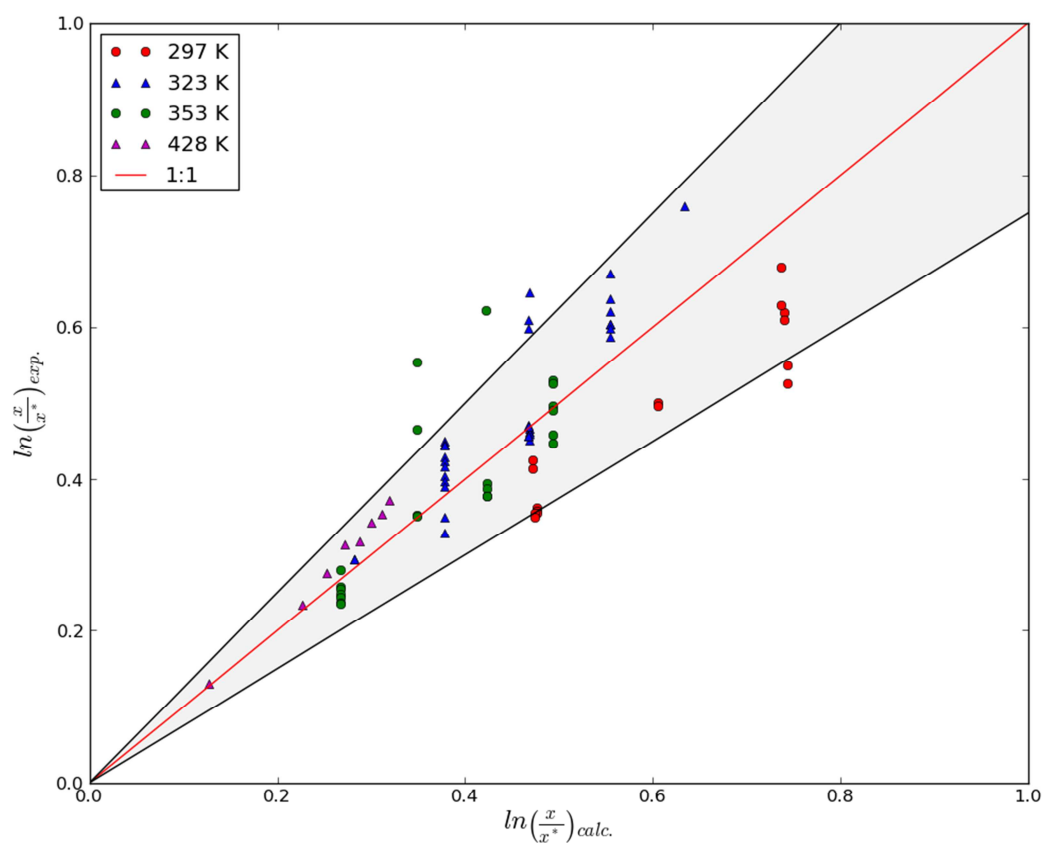
Figure 2. Ratio of H$_2$S solubility in pure water *x* and in aqueous NaCl solution *x** as a function of NaCl concentration at 298.15 K (red circles)(Barrett et al., 1988), 333.15 K (blue triangles) (Barrett et al., 1988; Xia et al., 2000), 353.15 K (green circles)(Barrett et al., 1988) and 428.15 K (pink triangles)(Suleimenov and Krupp, 1994). The shaded grey area corresponds to a relative uncertainty of ±25 %.
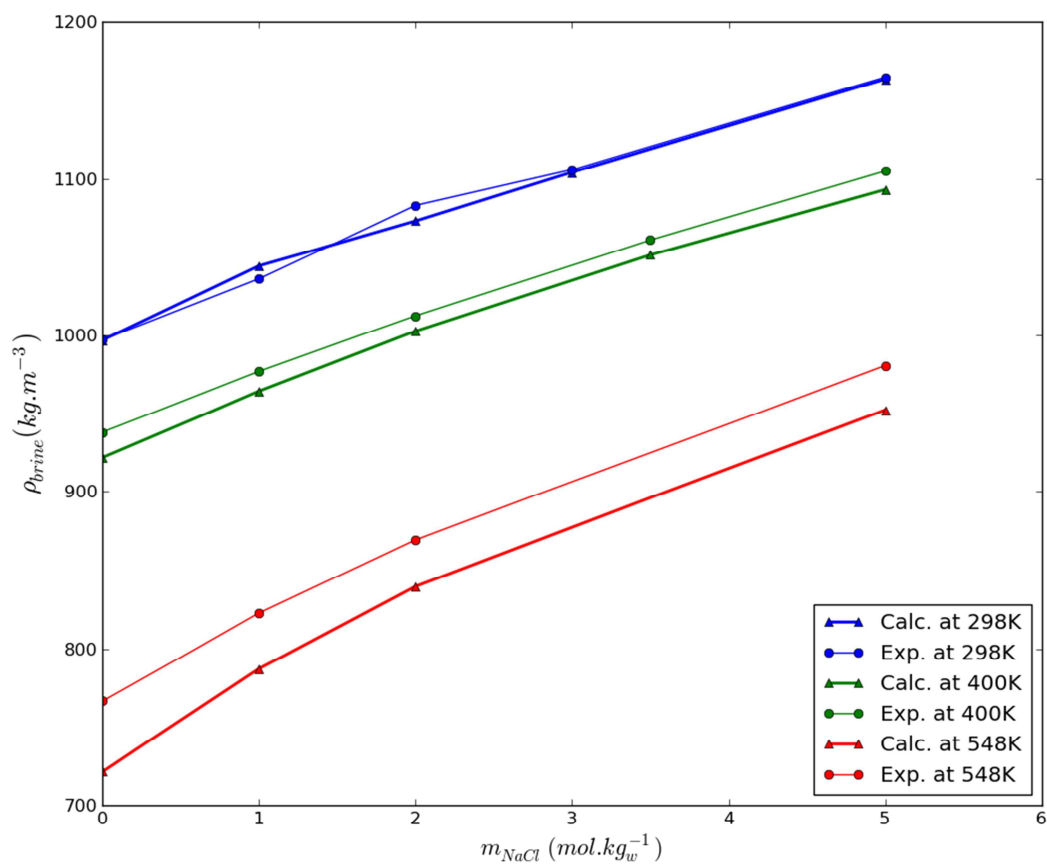
Figure 3. Experimental (circles) (Apelblat and Manzurola, 1999; Zhang and Han, 1996) and calculated (triangles) liquid density of NaCl aqueous solution at 298 K, 400 K and 548 K.
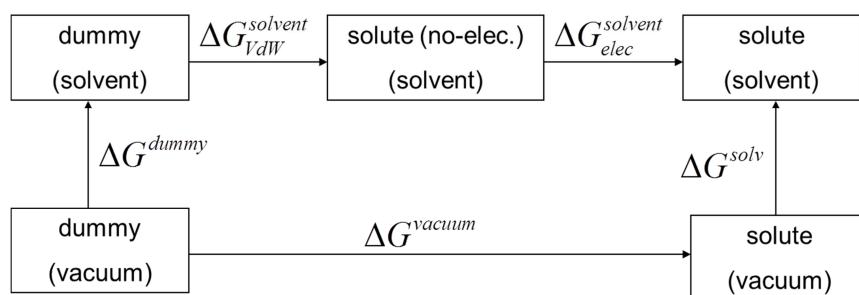
Figure 4. Thermodynamic cycle used to calculate Gibbs energy of solvation.
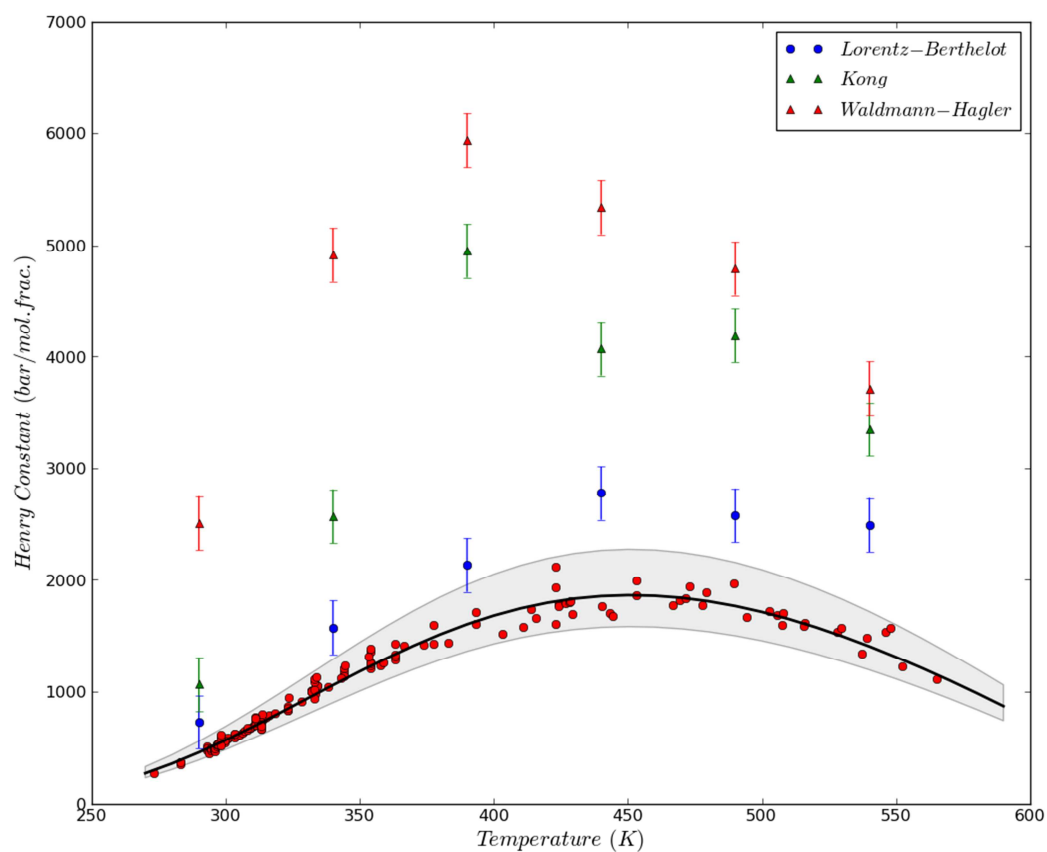
Figure 5. Henry constant of H_2S in pure water: experimental data (red symbols) and correlated (bold line) Henry constants of H_2S in pure water; the shaded grey area highlights the experimental uncertainties; Monte-Carlo simulation results with the combining rule of Lorentz-Berthelot, Kong and Waldmann-Hagler.
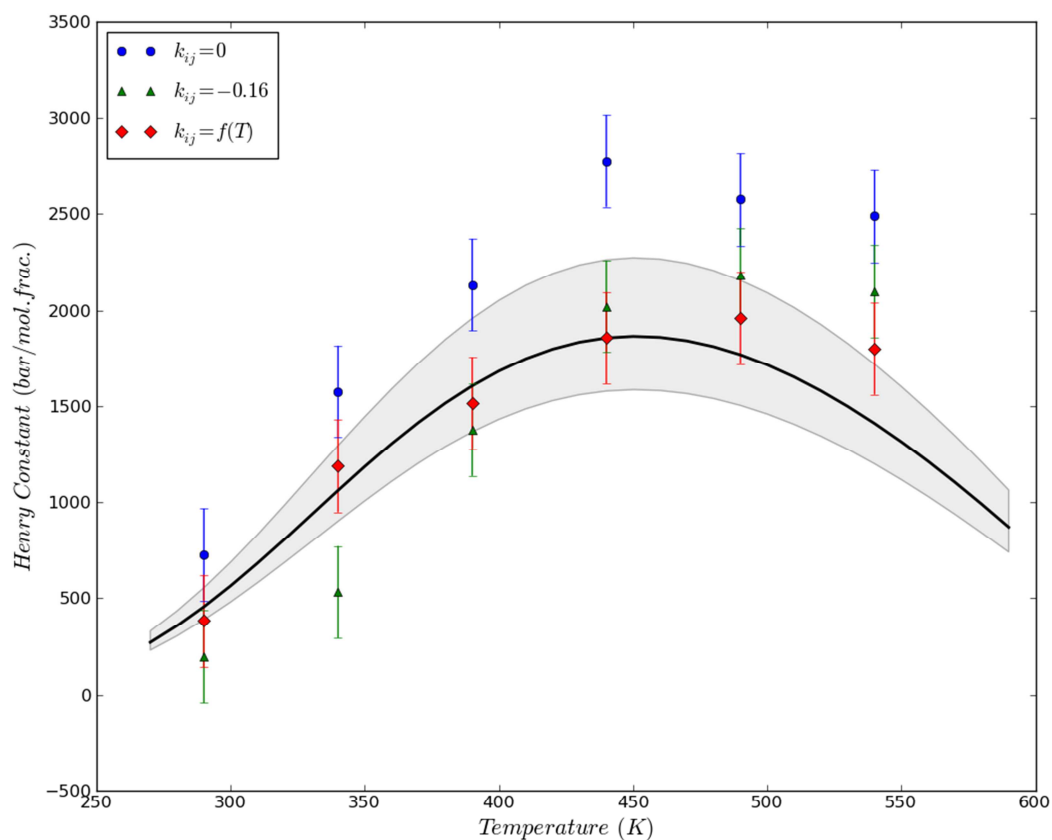
Figure 6. Henry constant of H₂S in pure water with the predictive approach (k_{ij}=0, circles), with the temperature-independent k_{ij} (k_{ij} =-0.16, green triangles), and with the temperature-dependent k_{ij} (equation
Error! Reference source not found.**, red triangles). The line represents the correlated experimental data, the shaded grey area highlights the experimental uncertainties.**
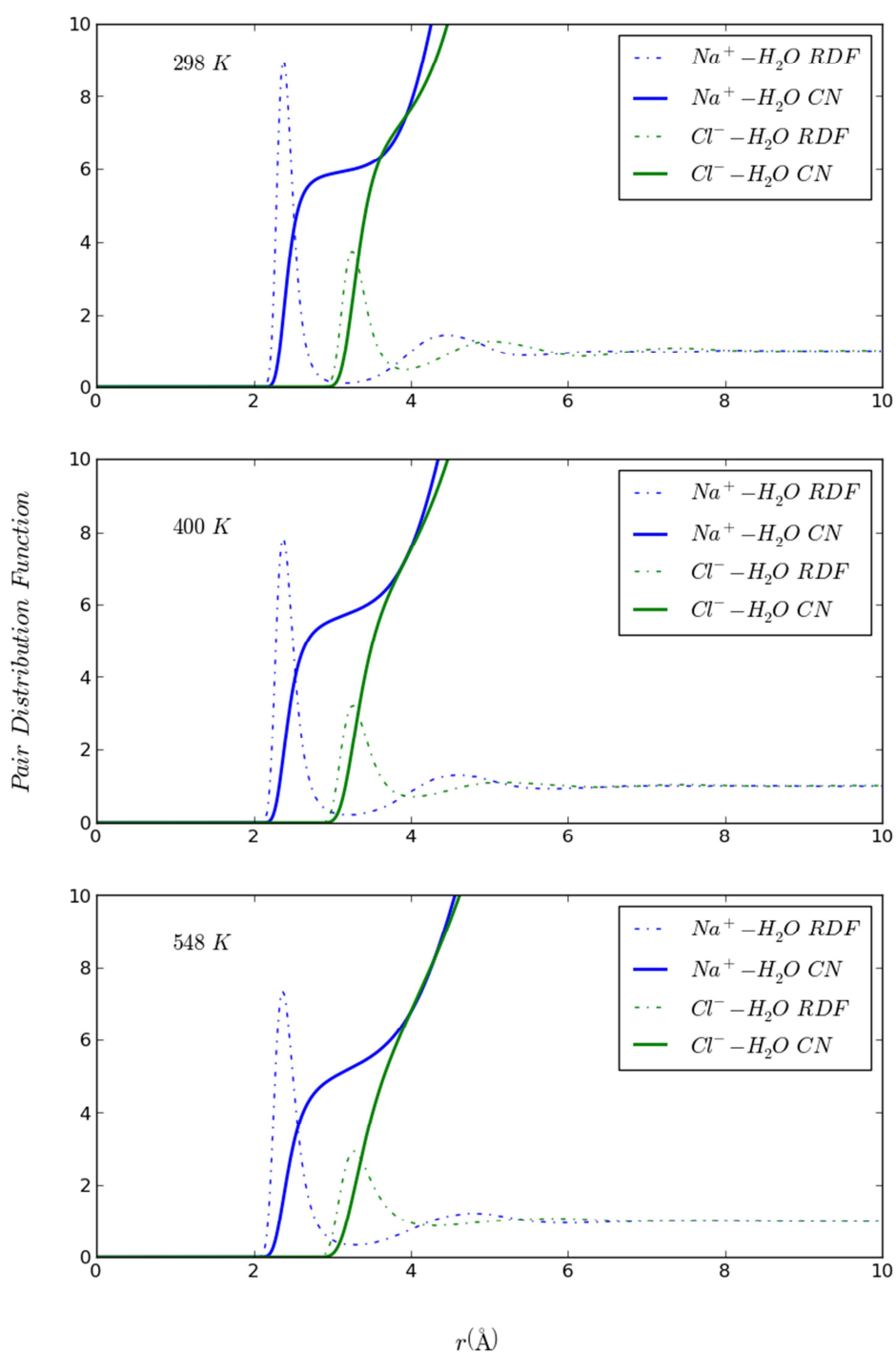
Figure 7. Radial distribution functions (RDF, dotted lines) and coordination numbers (CN, solid lines) for H₂O-Na⁺ pairs (in blue) and H₂O-Cl⁻ pairs (in green) in a NaCl aqueous solution at 1 mol/kg for three temperatures.
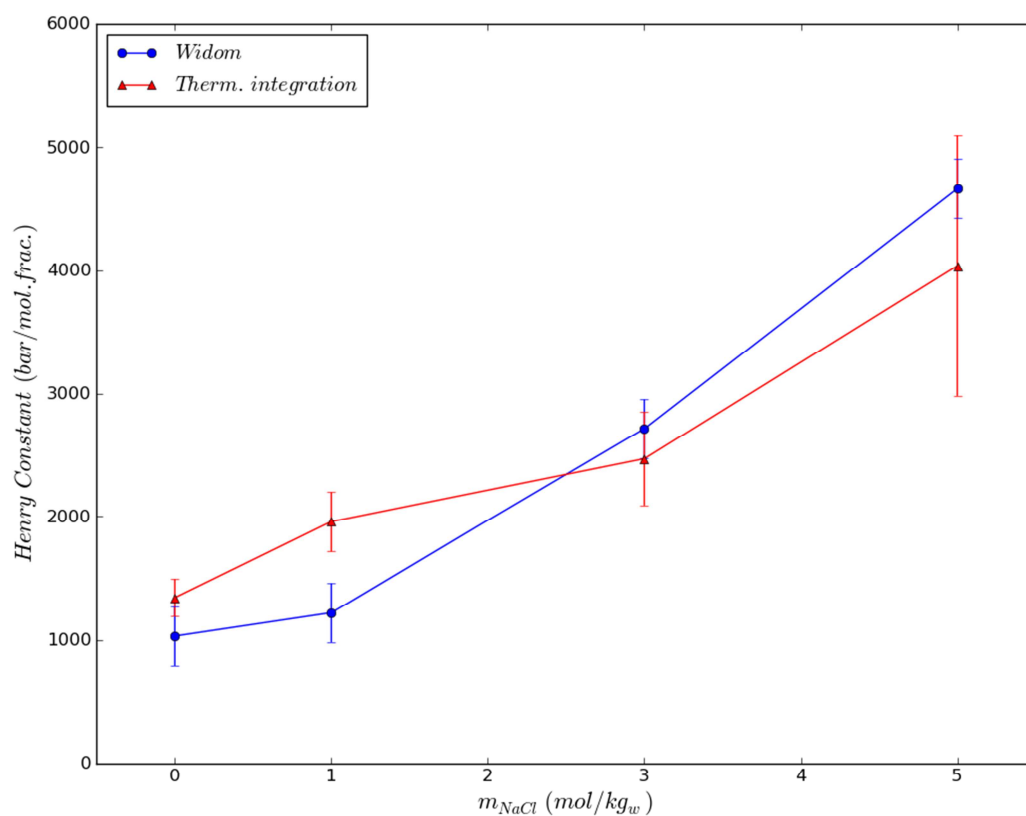
Figure 8. Henry constant of H$_2$S in aqueous NaCl solutions calculated at 323.15 K either with the Widom particle insertion method or with the thermodynamic integration method.
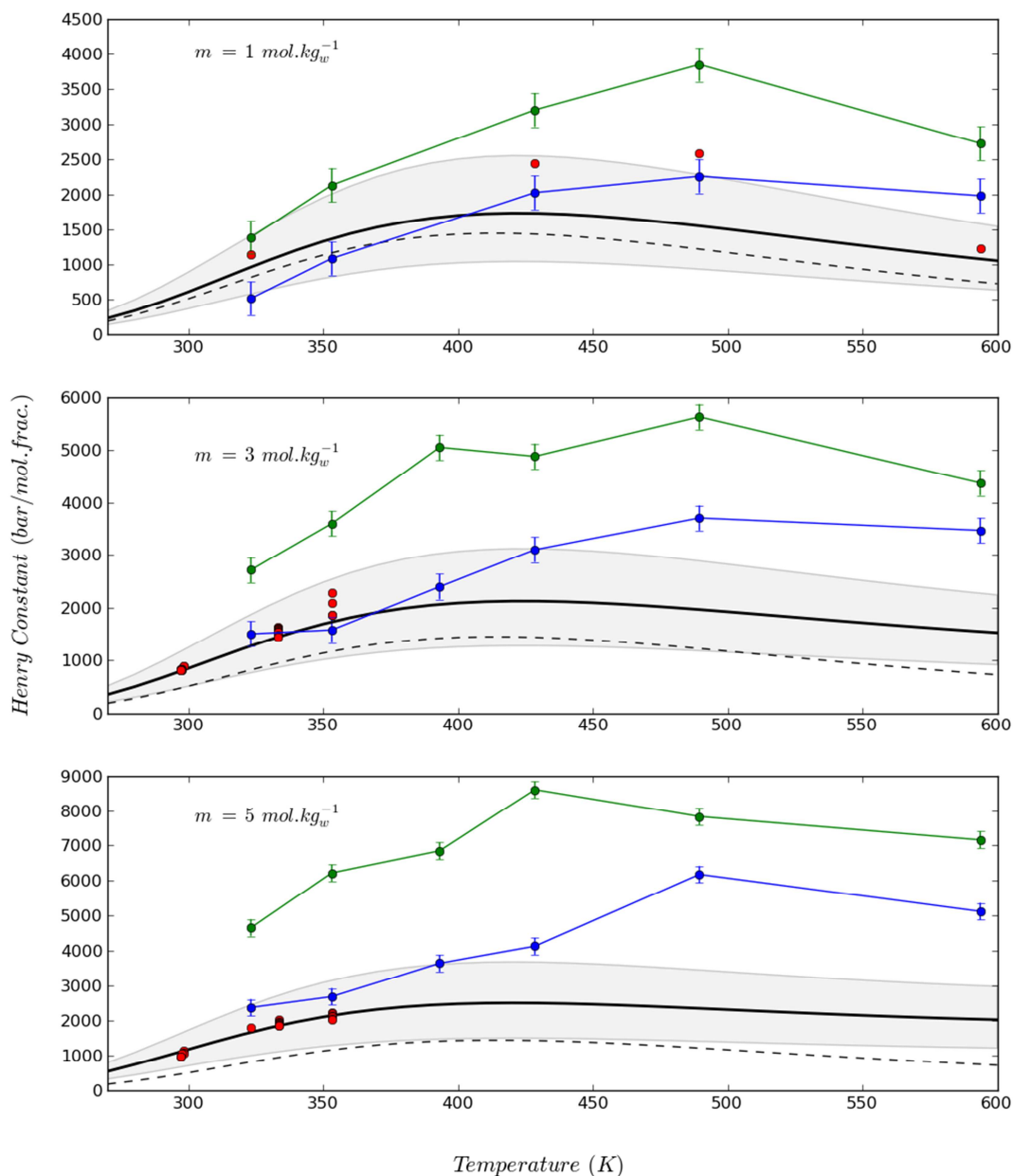
**Figure 9.** Henry constant of H_2S in NaCl aqueous solutions (1, 3, 5 mol/kg) as a function of the temperature. The Monte Carlo simulation results obtained with the predicted approach without k_{ij} are in green, while the ones obtained with the approach using the optimized H_2S-H_2O k_{ij} are in blue. For each molality, the available experimental data are plotted (red dots). The dash line is the correlated Henry constant of H_2S in pure water (eq. 2). The bold line is the correlated Henry constant of H_2S in aqueous solutions calculated according to the approach described in section 2.2. The shaded grey area shows the minimal uncertainty associated to the experimental measurements.

- Experimental Henry constants data of H_2S in NaCl aqueous solution are compiled from literature and smoothed with a simple correlation.
- A non-polarizable force field is evaluated to predict Henry constant of H_2S in NaCl aqueous solution through Monte Carlo simulations using Widom test insertion and thermodynamic integration methods.
- A temperature-independent interaction binary parameter is adjusted on experimental data and introduced in the force field.
- A good agreement between experimental and calculated Henry constant of H_2S in NaCl aqueous solution is obtained on a large temperature range (290 to 590 K) and salinity range (up to 6 mol/kg).